A Method to Estimate Synaptic Conductances From Membrane Potential Fluctuations

Michael Rudolph, Zuzanna Piwkowska, Mathilde Badoual, Thierry Bal, and Alain Destexhe
Integrative and Computational Neuroscience Unit (UNIC), Centre National de la Recherche Scientifique, 91198 Gif-sur-Yvette, France

Rudolph, Michael, Zuzanna Piwkowska, Mathilde Badoual, Thierry Bal, and Alain Destexhe. A method to estimate synaptic conductances from membrane potential fluctuations. *J Neurophysiol* 91: 2884–2896, 2004; 10.1152/jn.01223.2003. In neocortical neurons, network activity can activate a large number of synaptic inputs, resulting in highly irregular subthreshold membrane potential (V_m) fluctuations, commonly called "synaptic noise." This activity contains information about the underlying network dynamics, but it is not easy to extract network properties from such complex and irregular activity. Here, we propose a method to estimate properties of network activity from intracellular recordings and test this method using theoretical and experimental approaches. The method is based on the analytic expression of the subthreshold V_m distribution at steady state in conductance-based models. Fitting this analytic expression to V_m distributions obtained from intracellular recordings provides estimates of the mean and variance of excitatory and inhibitory conductances. We test the accuracy of these estimates against computational models of increasing complexity. We also test the method using dynamic-clamp recordings of neocortical neurons in vitro. By using an on-line analysis procedure, we show that the measured conductances from spontaneous network activity can be used to re-create artificial states equivalent to real network activity. This approach should be applicable to intracellular recordings during different network states in vivo, providing a characterization of the global properties of synaptic conductances and possible insight into the underlying network mechanisms.

INTRODUCTION

Neocortical neurons in vivo are characterized by intense subthreshold synaptic activity, which is often called "synaptic noise." This activity is particularly intense in activated states with desynchronized electroencephalogram (EEG), as expected from the high levels of firing (5–40 Hz) of cortical neurons during EEG-activated states (Evarts 1964; Steriade et al. 2001), combined with their remarkably dense level of interconnectivity (Braitenberg and Schüz 1998; DeFelipe and Fariñas 1992). The properties of synaptic noise during EEG-activated states were characterized by recent studies (Destexhe and Paré 1999; Paré et al. 1998), concluding that it is responsible for setting neocortical neurons into a "high-conductance state" (reviewed in Destexhe et al. 2003). The characteristics of high-conductance states are a depolarized membrane potential (V_m) of around −65 mV (≈15 mV depolarized with respect to rest), a 3- to 5-fold diminished input resistance, and high-amplitude V_m fluctuations (SD of the V_m of about $\sigma_v = 4$ mV).

Several types of computational models have been proposed to investigate high-conductance states. Biophysically detailed computational models can integrate the dendritic morphology of cortical neurons, and simulate active channels in soma and dendrites, as well as the large number of excitatory and inhibitory synapses underlying background activity (Bernander et al. 1991; Destexhe and Paré 1999; Rudolph and Destexhe 2003a). On the other hand, simplified models consider single compartments ("point-neurons") with global excitatory and inhibitory conductances (Destexhe et al. 2001). In this case, each global conductance represents the sum of a large number of individual synaptic inputs and is modeled by stochastic processes. The advantage of the latter approach is that the stochastic variations of synaptic conductances can be injected in real neurons to re-create high-conductance states in vitro, as shown in a number of recent studies (Chance et al. 2002; Destexhe et al. 2001; Fellous et al. 2003; Prescott and De Koninck 2003; Shu et al. 2003b) using the dynamic-clamp technique (Robinson and Kawai 1993; Sharp et al. 1993). These computational and dynamic-clamp approaches have shown that high-conductance states have a number of computational consequences on cortical neurons (reviewed in Destexhe et al. 2003). The stochastic and intense synaptic activity enhances their responsiveness (Hô and Destexhe 2000), modulates their gain (Chance et al. 2002; Fellous et al. 2003; Shu et al. 2003), sharpens the temporal processing of inputs (Bernander et al. 1991; Shelley et al. 2002; Shu et al. 2003b), or equalizes synaptic efficacies (Rudolph and Destexhe 2003a).

Another consequence of high-conductance states is that the subthreshold activity of any single neocortical neuron contains a large amount of information about the rest of the network. This is attributed to the particularly high level of firing activity of cortical neurons (see above), together with the dense intracortical connectivity (5,000 to 60,000 excitatory synapses per neuron; see DeFelipe and Fariñas 1992). Thus, neocortical neurons should provide a good "sampling" of the activity of a large number of neurons in the network, as indeed shown by the tight correlation between EEG and intracellular activity in cortex (Contreras and Steriade 1995; Creutzfeldt et al. 1996a,b; Klee et al. 1965). In principle it should be possible to deduce properties of network activity by analyzing the subthreshold dynamics of the V_m, but unfortunately no such methods are yet available. The main difficulty is to relate collective properties at the network level into identifiable patterns of synaptic activity. At present, only global characterizations are possible, such as for example characterizing the mean rate of firing of the excitatory and inhibitory cells, which should translate into

Address for reprint requests and other correspondence: A. Destexhe, Integrative and Computational Neuroscience Unit (UNIC), CNRS, 1 Ave. de la Terrasse (Bat. 33), 91198 Gif-sur-Yvette, France (E-mail: Destexhe@iaf.cnrs-gif.fr).

the mean value of global excitatory and inhibitory conductances. Interestingly, the variance of global synaptic conductances is related to the average amount of correlation present among presynaptic neurons (Destexhe et al. 2001), but it is presently very difficult to estimate the variance of conductances.

A possible path toward such a characterization is to obtain a good mathematical description of the dynamics of synaptic noise, and deduce useful relations between the V_m dynamics and presynaptic activity. However, the mathematical description must not be too complex, to allow inverting the relations and obtain characteristics of network activity as a function of V_m measurements. This is the approach that we follow in this paper. We showed that by using stochastic calculus, one can obtain an analytical description of the steady-state V_m distribution (Rudolph and Destexhe 2003b). We use here the results of this theoretical approach to analyze the V_m activity of cortical neurons. The method of analysis we propose is tested against computational models of increasing complexity, as well as in real neurons during active states in vitro. Part of these results have appeared in 2 conference abstracts (Destexhe et al. 2003; Rudolph and Destexhe 2002).

METHODS

Models of cortical neurons and synaptic noise

To reproduce the stochastic membrane potential fluctuations and high-conductance state characterizing the dynamics of neocortical neurons in vivo, several types of neuronal models were used and compared (see Fig. 1).

Effective point-conductance model

The first model was a *point-conductance* model (Destexhe et al. 2001), which consisted in a single-compartment neuron described by the passive stochastic membrane equation

$$C_m \frac{dV(t)}{dt} = g_L[E_L - V(t)] - \frac{1}{a}I_{syn}(t) + \frac{1}{a}I_{ext} \qquad (1)$$

where $V(t)$ is the membrane potential, a is the membrane area, C_m is the specific membrane capacitance, and g_L and E_L are the leak conductance density and reversal potential, respectively. I_{ext} denotes a constant external (stimulating) current. Synaptic noise is described by the total synaptic current $I_{syn}(t)$, which was decomposed into a sum of 2 independent current terms

$$I_{syn}(t) = g_e(t)[V(t) - E_e] + g_i(t)[V(t) - E_i] \qquad (2)$$

where $g_e(t)$ and $g_i(t)$ are time-dependent global excitatory and inhibitory conductances, respectively, and E_e and E_i are their respective reversal potentials. $g_e(t)$ and $g_i(t)$ were described by one-variable stochastic processes similar to the Ornstein–Uhlenbeck process (Uhlenbeck and Ornstein 1930)

$$\frac{dg_{\{e,i\}}(t)}{dt} = -\frac{1}{\tau_{\{e,i\}}}[g_{\{e,i\}}(t) - g_{\{e,i\}0}] + \sqrt{\frac{2\sigma_{\{e,i\}}^2}{\tau_{\{e,i\}}}}\chi_{\{e,i\}}(t) \qquad (3)$$

where g_{e0} and g_{i0} are average conductances, τ_e and τ_i are time constants, σ_e and σ_i are noise SD values, and $\chi_e(t)$ and $\chi_i(t)$ denote independent Gaussian white noise processes of unit SD and zero mean.

The model was accessed both analytically and numerically. In the latter case, the membrane area of the compartment was $a = 34,636$ μm^2 (corresponding to the layer VI neocortical pyramidal cells from

cat parietal cortex used in Destexhe et al. 2001), and passive parameters were $g_L = 0.0452$ mS/cm^2, $E_L = -80$ mV, $C_m = 1$ $\mu F/cm^2$ (Destexhe and Paré 1999; Paré et al. 1998), $E_e = 0$ mV and $E_i = -75$ mV. Other synaptic noise parameter values were chosen to obtain an average membrane potential of about -65 mV with SD around 4 mV characteristic for in vivo states of cortical neurons (Destexhe and Paré 1999; Paré et al. 1998), and were $g_{e0} = 12.1$ nS, $g_{i0} = 57.3$ nS, $\sigma_e = 12$ nS, $\sigma_i = 26.4$ nS, $\tau_e = 2.73$ ms, and $\tau_i = 10.49$ ms.

Simulations of the point-conductance model and its comparison with more complex models are illustrated in Fig. 1. The point-conductance model (Fig. 1A) generates irregular subthreshold activity consistent with in vivo measurements (Destexhe et al. 2001). It is characterized by a Lorentzian power spectrum (Fig. 1C, dashed lines), as well as by a symmetric (Gaussian) distribution of excitatory and inhibitory conductances (Fig. 1D, dashed lines), resulting in a nearly symmetric amplitude distribution of the membrane potential V_m (Fig. 1E, dashed lines).

Single-compartment model with individual noise sources

The second model consisted in a single-compartment membrane with a more realistic representation of synaptic inputs, which were modeled by a large number of individual synaptic conductances. In this case, the synaptic current $I_{syn}(t)$ in *Eq. 1* was described by

$$I_{syn}(t) = \sum_{n=1}^{N} g_{AMPA}m_e^{(n)}(t)(V - E_e) + \sum_{m=1}^{M} g_{GABA}m_i^{(m)}(t)(V - E_i) \qquad (4)$$

where N and M denote the total number of excitatory and inhibitory synapses, modeled by α-amino-3-hydroxy-5-methyl-4-isoxazolepropionic (AMPA) and γ-aminobutyric acid (GABA) postsynaptic receptors (Destexhe et al. 1998) with quantal conductances g_{AMPA} and g_{GABA}, respectively. $m_e^{(j)}(t)$ and $m_i^{(k)}(t)$ represent the fractions of postsynaptic receptors in the open state at each individual synapse, and were described by the following kinetic equations

$$\frac{dm_{\{e,i\}}}{dt} = \alpha_{\{e,i\}}[T](t)(1 - m_{\{e,i\}}) - \beta_{\{e,i\}}m_{\{e,i\}} \qquad (5)$$

where $[T](t)$ is the transmitter concentration in the cleft, $\alpha_{\{e,i\}}$ and $\beta_{\{e,i\}}$ are respectively forward and backward binding rate constants for excitation (index e) and inhibition (index i). When a spike occurred in the presynaptic compartment, a pulse of transmitter was triggered such that $[T] = T_{max}$ for a short time period t_{dur} and $[T] = 0$ until the next release occurs. These kinetic models of synaptic currents were as described previously (Destexhe et al. 1998), with kinetic parameters that were obtained by fitting the model to postsynaptic currents recorded experimentally. To simulate synaptic background activity, all synapses were activated randomly according to independent Poisson processes with mean rates of ν_{exc} and ν_{inh} for AMPA and GABA$_A$ synapses, respectively. The activation of N-methyl-D-aspartate (NMDA) receptors is minimal at the subthreshold levels investigated here, and were not included for simplicity.

The model was simulated numerically with passive properties as in the point-conductance model. Synaptic parameters were $N = 4,472$, $M = 3,801$, $g_{AMPA} = 1,200$ pS, $g_{GABA} = 600$ pS, $\alpha_e = 1.1 \times 10^6$ M^{-1} s^{-1}, $\beta_e = 670$ s^{-1} for AMPA receptors, $\alpha_i = 5 \times 10^6$ M^{-1} s^{-1}, $\beta_i = 1\,80$ s^{-1} for GABA$_A$ receptors, $T_{max} = 1$ mM, $t_{dur} = 1$ ms, $\nu_{exc} = 2.16$ Hz, and $\nu_{inh} = 2.4$ Hz.

Simulations of this model are illustrated in Fig. 1B. The power spectra of the total excitatory and inhibitory conductances are approximately Lorentzian (Fig. 1C, gray), whereas their amplitude distributions take a nearly symmetric (Gaussian) shape (Fig. 1D, gray). Also the V_m amplitude distribution follows an approximately symmetric behavior (Fig. 1E, gray). It is to be noted that the point-conductance model captures these properties remarkably well (compare gray areas with dashed lines in Fig. 1, C–E), thus suggesting that the Ornstein–
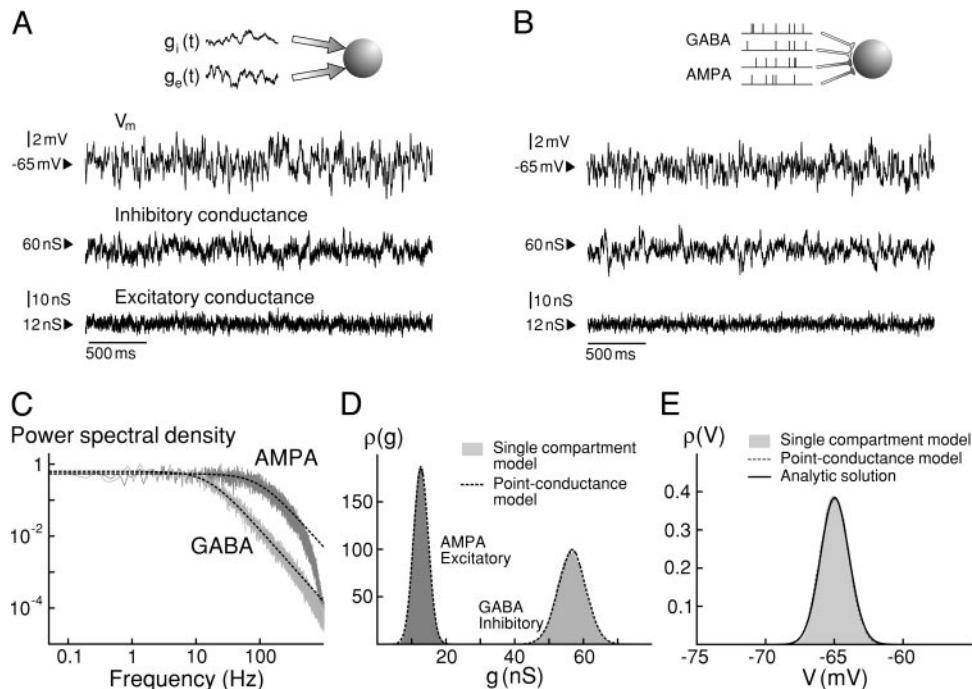
FIG. 1. Detailed and simplified models of synaptic background activity. *A*: point-conductance model of synaptic background activity. Synaptic background activity was produced by 2 global excitatory and inhibitory conductances (g_e and g_i in *top scheme*), which were simulated by stochastic models (see Destexhe et al. 2001). Traces show, respectively, the membrane potential (V_m) as well as the total excitatory (g_e) and inhibitory (g_i) conductances resulting from synaptic bombardment. *B*: synaptic background activity in a single-compartment model of a cortical neuron with realistic synaptic inputs. Synaptic activity was simulated by the random release of a large number of excitatory and inhibitory synapses (4,472 and 3,801 synapses, respectively; see *top scheme*). Individual synaptic currents were described by kinetic models of glutamate (AMPA) and GABAergic (GABA$_A$) receptors. Traces show, respectively the V_m, total excitatory and inhibitory conductances as in *A*. *C*: power spectral densities of the 2 models (dashed lines: point-conductance model as in *A*, gray: single compartment model as in *B*). *D*: distribution of synaptic conductances $\rho(g_e)$ and $\rho(g_i)$ (gray: point-conductance model; dashed lines: single-compartment model). *E*: membrane potential distribution $\rho(V)$ (gray: point–conductance model; dashed lines: single-compartment model). Solid line indicates the analytic expression for the V_m distribution, as obtained from solving the Fokker–Planck equation for the point-conductance model. Panels *C* to *E* show that the 2 models share similar statistical properties, but the point-conductance model in *B* is more than 2 orders of magnitude faster to simulate.

Uhlenbeck stochastic process yields a valid description of synaptic noise.

Detailed biophysical model

The third model consisted in a compartmental model of a neocortical layer VI pyramidal neuron obtained from morphological reconstructions of cells recorded in cat association cortex (Contreras et al. 1997). The passive properties (see point-conductance model) were adjusted by matching the model to intracellular recordings obtained in the absence of synaptic activity (Destexhe and Paré 1999). In some cases, voltage-dependent conductances were inserted in the soma, dendrites, and axon and were described by Hodgkin and Huxley (1952) type models. The latter model included 2 voltage-dependent currents, a fast Na$^+$ current I_{Na}, and a delayed-rectifier K$^+$ current I_{Kd}, for action potential generation (Traub and Miles 1991) with conductance densities of 8.4 and 7 mS/cm^2 (Huguenard et al. 1988; densities were 10 times higher in the axon), respectively. To account for the spike-frequency adaptation and afterhyperpolarization commonly observed in "regular-spiking" neurons, a slow voltage-dependent K$^+$ current I_M (muscarinic potassium current; Gutfreund et al. 1995) with conductance densities of 0.35 mS/cm^2 (soma and dendrites, no I_M in axon) was added. In some simulations, models of cortical neurons with additional fast inactivating A-type K$^+$ current I_{KA} (model from Migliore et al. 1999; conductance density from Bekkers 2000), T-type (low threshold) Ca^{2+} current I_{CaT} (model from Traub et al. 2003; conductance density from Hamill et al. 1991) and

hyperpolarization-activated current I_h (model and nonuniform conductance density from Stuart and Spruston 1998) were used.

To simulate synaptic inputs, pyramidal cells were divided into different regions (soma, perisomatic dendrites, main dendrites, axon initial segment) and the density of AMPA and GABA$_A$ synapses in each region was estimated from morphological studies (see DeFelipe and Fariñas 1992; for kinetic parameters see single-compartment model with individual noise sources). The number of synapses per 100 μm^2 of membrane were: 10–20 (GABA$_A$, soma and perisomatic dendrites), 40–80 (GABA$_A$, axon initial segment), 8–12 (GABA$_A$, dendrites), and 55–65 (AMPA, dendrites), leading to a total of $N = 16,563$ glutamatergic and $M = 3,376$ GABAergic synapses. Synaptic currents were simulated by kinetic models of AMPA and GABA$_A$ receptor types as described above, and synaptic background activity was simulated by random (Poisson-distributed) synaptic events at a mean rate of $\nu_{exc} = 1$ Hz and $\nu_{inh} = 5.5$ Hz for AMPA and GABA$_A$ synapses, respectively. This model was described in detail in a previous study (Destexhe and Paré, 1999).

To estimate the conductances underlying synaptic activity, as well as their variances, we followed a procedure identical to that of a previous paper (Destexhe et al. 2001). An "ideal" voltage clamp (without electrode series resistance) was simulated using a somatic electrode. The model was run twice at 2 different clamped voltages (-65 and -55 mV), and using the same random seed (so that the same random numbers were used at each clamp). The leak-subtracted currents obtained were then decomposed into excitatory and inhibitory conductances using the relation

$$I(t) = g_e(t)(V_c - E_e) + g_i(t)(V_c - E_i) \qquad (6)$$

where V_c is the clamped voltage. This procedure yields "effective" global synaptic conductances [$g_e(t)$, $g_i(t)$] as seen from a somatic electrode.

All simulations were performed using the NEURON simulation environment (Hines and Carnevale 1997) and were run on PC-based workstations under the Linux operating system.

In vitro experiments

In vitro experiments were performed on 0.4-mm-thick coronal or sagittal slices from the lateral portions of the ferret occipital cortex including primary and secondary (areas 17, 18, and 19) visual cortical areas. Ferrets, 4–12 mo old (Marshall Europe, Lyon), were anesthetized with sodium pentobarbital (30 mg/kg). The slices were maintained in an interface-style recording chamber at 35–36°C. Slices were prepared on a DSK microslicer (Ted Pella, Redding, CA) in a slice solution in which the NaCl was replaced with sucrose while maintaining an osmolarity of 307 mOsm. After transfer to the recording chamber, the slices were incubated in slice solution containing (in mM): NaCl, 124; KCl, 2.5; $MgSO_4$, 2; $NaHPO_4$, 1.25; $CaCl_2$, 2; $NaHCO_3$, 26; dextrose, 10, and was aerated with 95% O_2-5% CO_2 to a final pH of 7.4. After about 1 h, the slice solution was modified to contain 1 mM $MgCl_2$, 1 or 1.2 mM $CaCl_2$, and 3.5 mM KCl (Sanchez-Vives and McCormick 2000). Intracellular recordings after 2 h of recovery were performed in deep layers (layers IV, V, and VI) on electrophysiologically identified regular spiking and intrinsically bursting cells. Electrodes for intracellular recordings were made on a Sutter Instruments P-87 micropipette puller from medium-walled glass (WPI, 1BF100) and beveled on a Sutter Instruments beveler (BV-10M). Micropipettes were filled with 1.2 to 2 M potassium acetate and had resistances of 80–100 MΩ after beveling.

Ferret visual cortical slices spontaneously display recurrent periods of activity lasting 0.5–1.5 s, which are separated by periods of quiescence lasting 2–20 s (Sanchez-Vives and McCormick 2000). In intracellular recordings, this active network activity manifests as a depolarized state ("up-state"). During the periods of quiescence ("down-state"), the membrane potential relaxes toward its resting value. To characterize synaptic noise, intracellular recordings in up- and down-states were collected at several different membrane potentials maintained by injection of steady currents through the recording micropipette (current-clamp).

Dynamic-clamp experiments

The dynamic-clamp technique (Robinson et al. 1993; Sharp et al. 1993) was used to inject computer-generated conductances in real neurons. Dynamic-clamp experiments were run using the hybrid RT-NEURON environment (developed by G. Le Masson, INSERM U378, Université de Bordeaux), which is a modified version of NEURON (Hines and Carnevale 1997) running under the Windows NT 4.0 operating system (Microsoft) on a PC equipped with a 1.4-GHz Pentium IV processor. NEURON was augmented with the capacity of simulating neuronal models in real time, synchronized with the intracellular recording. To achieve real-time simulations as well as data transfer to the PC for further analysis, we used a PCI DSP board (Innovative Integration, Simi Valley, CA) with 4 analog/digital (inputs) and 4 digital/analog (outputs) 16 bits converters. The DSP board constraints calculations of the models and data transfer process to be made with a high priority level by the PC processor. The DSP board allows input (e.g., the membrane potential of the real cell incorporated in the equations of the models) and output signals (the synaptic current to be injected into the cell) to be processed at regular intervals (time resolution = 0.1 ms). A custom interface was used to connect the digital and analog inputs/outputs signals of the DSP board with the intracellular amplifier (Axoclamp 2B, Axon Instruments) and the data

acquisition systems (PC-based acquisition software ELPHY, developed by G. Sadoc, CNRS Gif-sur-Yvette, ANVAR, and Biologic). The dynamic-clamp protocol was used to insert the fluctuating conductances underlying synaptic noise in cortical neurons using the point-conductance model, similar to a previous study (Destexhe et al. 2001). A critical feature for dynamic clamp and for the present method is the accuracy of the absolute membrane voltage measure. A reliable method is to monitor and adjust manually the V_m offset during the course of the recording according to the known statistical value of the onset of action potentials in a given cell type (e.g., −55 mV for ferret pyramidal cells; Shu et al. 2003b). For this purpose, action potentials are triggered by square depolarizing pulses of current injected through the micropipette.

Data acquisition and analysis

Voltage traces from numerical simulations and experimental recordings were analyzed with respect to both their statistical properties and amplitude distribution $\rho(V)$. In models, simulations were run using either passive models or models with active currents responsible for spike generation and adaptation (see above). In experiments, spontaneous up-states were collected using custom data acquisition software (ELPHY). In all cases, the data acquisition rate was 100 kHz (numerical simulations) or 20 kHz (experiments). To obtain sub-threshold V_m distributions, steady hyperpolarizing current was used such that the average V_m in up-states was between −75 and −65 mV. The remaining action potentials, if present, were cut using a time window of 10 ms centered around the spike (taking advantage of the fact that signals need not to be contiguous to calculate amplitude distributions).

V_m distributions were calculated using bin sizes of 0.2 mV for traces from both simulations and experiments. The distributions obtained were fitted using a Gaussian template function (e.g., Eq. A6 in the APPENDIX), thereby providing directly the values for the average V_m, $\bar{V}$, and its SD, σ_V. These estimates were also checked with standard statistical analysis tools for discrete data sets (Press et al. 1993).

To calculate these values from the analytic expressions of $\rho(V)$, which usually do not allow explicit integration, we integrated $\rho(V)$ numerically, using

$$\bar{V} = \int_{-\infty}^{\infty} dV V \rho(V) \qquad (7)$$

$$\sigma_V^2 = \int_{-\infty}^{\infty} dV(V - \bar{V})^2 \rho(V) \qquad (8)$$

for the mean and SD of the voltage distributions, respectively.

Finally, the effective membrane area (a) and the leak conductance density (g_L) can be estimated from experimental data by using injection of hyperpolarizing current pulses during periods of quiescent activity, yielding estimates of the membrane time constant (τ_m) and of the resting input resistance (R_{in}). g_L and a can be estimated using the following relations

$$1/R_{in} = ag_L \quad \tau_m = g_L/C_m$$

assuming a fixed value for C_m (1 $\mu F/cm^2$). Note that this procedure for estimating g_L may be a potential source of error because even during periods of quiescent network activity, the membrane still receives background synaptic inputs (e.g., residual network activity or miniature synaptic events). Ideally, synaptic currents should be blocked pharmacologically to faithfully estimate g_L. However, this procedure is technically difficult, in particular during feedback experiments where the same cell is used for analyzing and re-creating high-conductance states (see RESULTS), and was therefore not attempted here.

RESULTS

We start by outlining the procedure used for estimating synaptic conductances from membrane potential (V_m) amplitude distributions. We next test this procedure against models of increasing complexity. Finally, we demonstrate the application of this approach to in vitro experiments and test the results obtained using dynamic clamp.

The VmD method: estimating synaptic conductances from membrane potential distributions

We consider the V_m probability density function $\rho(V, t)$ of the point-conductance model defined in *Eqs. 1–3*. $\rho(V, t)$ describes the probability density that the membrane potential V_m takes the value V at time t. The time evolution of this probability density function is given by the *Fokker–Planck equation* (Risken 1984; see APPENDIX), which for the point-conductance model yields the following steady-state solution (Rudolph and Destexhe 2003b)

$$\rho(V) \approx \exp\{A_1\ln[B_1(V - E_e)^2 + B_2(V - E_i)^2]$$
$$+ A_2\arctan[B_3(V - E_e) + B_4(V - E_i)]\} \quad (9)$$

where A_i and B_j are voltage-independent terms depending on passive membrane and synaptic noise parameters (see *Eq. A4* in the APPENDIX for full expression).

This analytic expression for the V_m distribution was derived and analyzed in detail in a previous study (Rudolph and Destexhe 2003b). Here we focus on possible applications of this analytic approach to analyze subthreshold neuronal activity from current-clamp recordings. The general idea is to fit analytic expressions of the V_m distribution to distributions obtained experimentally, thereby providing estimates of the underlying conductance parameters, which characterize network activity.

Although this estimate could in principle be obtained by fitting *Eq. 9* to experimentally measured V_m distributions, in practice, this approach poses a number of problems. The main obstacle is the highly nonlinear dependency of the the V_m distribution on its parameters (*Eq. 9*). In general, fitting a highly nonlinear function of many parameters to experimental data results in local minima that may lead to spurious estimates (Press et al. 1993). To circumvent this difficulty, we need to simplify *Eq. 9*. Here, we can take advantage of the fact that the V_m distribution is only weakly asymmetric in V, especially in the range of V_m values typical of in vivo activity (-70 to -50 mV; see detailed analysis in Rudolph and Destexhe 2003b). Furthermore, a very convenient symmetric approximation of *Eq. 9* can be obtained and takes the form of a Gaussian distribution

$$\rho(V) \approx \exp\left[- \frac{(V - \bar{V})^2}{2\sigma_V^2} \right] \quad (10)$$

where $\bar{V}$ is the average V_m and σ_V is the standard deviation of the V_m. This Gaussian approximation can be obtained formally from *Eq. 9* by second-order Taylor expansion around its peak value (see details in the APPENDIX). As we will see below, this expression provides an excellent approximation of the V_m distributions obtained from models and experiments.

The advantage of using a simplified expression such as *Eq. 10* is 2-fold. First, one can obtain an expression of the quantities $\bar{V}$ and σ_V (very easy to measure in experiments) as a function of the synaptic conductance parameters (see *Eqs. A5 and A7* in the APPENDIX), which allows physical interpretation of these quantities. For example, it can be seen that $\bar{V}$ is mostly determined by the static components of the synaptic conductances (g_{e0} and g_{i0}), whereas σ_V has a more complex dependency on synaptic noise parameters. It depends on both g_{e0} and g_{i0}, as well as on σ_e and σ_i.

The second and main advantage is that these expressions are mathematically simple enough to enable inverting them, which may lead to expressions of the synaptic noise parameters as a function of the V_m measurements, $\bar{V}$ and σ_V. The stochastic passive membrane equation, *Eq. 1*, is characterized by 6 parameters describing excitatory and inhibitory conductance noise ($g_{e0}, g_{i0}, \sigma_e, \sigma_i, \tau_e, \tau_i$). Two of these parameters, the noise time constants τ_e and τ_i, are related to the decay time of synaptic currents and thus the kinetics of synaptic transmission. Therefore, these parameters are expected to show little variations from cell to cell, and can be fixed using power spectra of synaptic conductances deduced from voltage-clamp recordings (see Destexhe et al. 2001). In contrast, the remaining 4 parameters, the means (g_{e0}, g_{i0}) and SDs (σ_e, σ_i) of excitatory and inhibitory synaptic conductances, depend on the synaptic inputs converging to the cell as well as the actual network state. Thus these parameters are expected to vary from one situation to the other (e.g., between different network states), as well as from cell to cell (e.g., depending on the connectivity of that particular cell within the network), and should therefore be estimated for each case.

To extract the 4 conductance parameters ($g_{e0}, g_{i0}, \sigma_e, \sigma_i$) from the membrane probability distribution, *Eq. 10* is, however, insufficient because it is characterized by only 2 parameters ($\bar{V}, \sigma_V$). To solve this problem, one possibility is to consider 2 V_m distributions obtained at 2 different constant levels of injected current I_{ext1} and I_{ext2} (2 current-clamps protocol). In this case, expressing these 2 V_m distributions as *Eq. 10* leads to 2 values for mean V_m, $\bar{V}_1$ and $\bar{V}_2$, as well as 2 values for the V_m SD, σ_{V1} and σ_{V2}. If both distributions are obtained during the same network state, they can be expressed (using *Eqs. A5 and A7* in the APPENDIX) as a function of the same 4 parameters ($g_{e0}, g_{i0}, \sigma_e, \sigma_i$). In this case, one obtains

$$g_{\{e,i\}0} = \frac{(I_{ext1} - I_{ext2})[\sigma_{V_2}^2(E_{\{i,e\}} - \bar{V}_1)^2 - \sigma_{V_1}^2(E_{\{i,e\}} - \bar{V}_2)^2]}{[(E_e - \bar{V}_1)(E_i - \bar{V}_2) + (E_e - \bar{V}_2)(E_i - \bar{V}_1)](E_{\{e,i\}} - E_{\{i,e\}})(\bar{V}_1 - \bar{V}_2)^2}$$
$$- \frac{(I_{ext1} - I_{ext2})(E_{\{i,e\}} - \bar{V}_2) + [I_{ext2} - g_L a(E_{\{i,e\}} - E_L)](\bar{V}_1 - \bar{V}_2)}{(E_{\{e,i\}} - E_{\{i,e\}})(\bar{V}_1 - \bar{V}_2)} \quad (11)$$

$$\sigma_{\{e,i\}}^2 = \frac{2aC_m(I_{ext1} - I_{ext2})[\sigma_{V_1}^2(E_{\{i,e\}} - \bar{V}_2)^2 - \sigma_{V_2}^2(E_{\{i,e\}} - \bar{V}_1)^2]}{\tilde{\tau}_{\{e,i\}}[(E_e - \bar{V}_1)(E_i - \bar{V}_2) + (E_e - \bar{V}_2)(E_i - \bar{V}_1)](E_{\{e,i\}} - E_{\{i,e\}})(\bar{V}_1 - \bar{V}_2)^2}$$
$$(12)$$

These relations enable us to estimate global characteristic of network activity, such as mean excitatory (g_{e0}) and inhibitory (g_{i0}) synaptic conductances, as well as their respective variances (σ_e^2, σ_i^2), from the sole knowledge of the V_m distributions obtained at 2 different levels of injected current. This procedure, which we refer to below as the "VmD method," is illustrated in Fig. 2 and constitutes the core of the analysis explored in this paper.

It is worth noting that the method can be generalized to various current levels. For one current level (one current-clamp
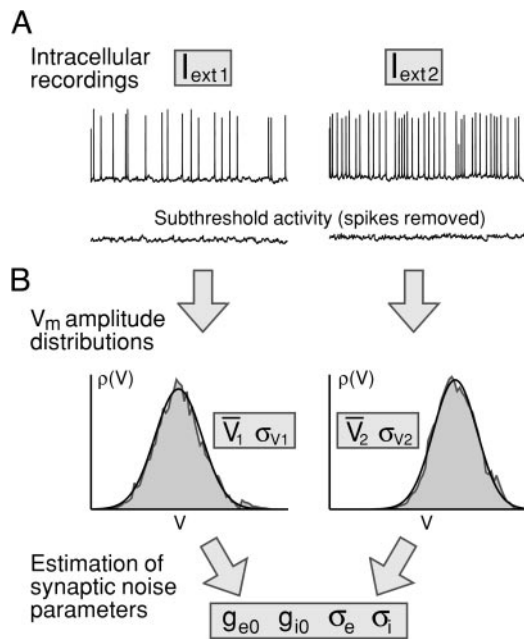
FIG. 2. Sketch of the VmD method to estimate synaptic conductances from membrane potential fluctuations. *A*: membrane potential recordings of network activity at 2 different current levels I_{ext1} and I_{ext2} (*top traces*). Spikes are removed (*bottom traces*) or the activity is recorded at hyperpolarized levels to yield subthreshold activity. *B*: computation of membrane potential distributions (gray) at these 2 current levels and fitting with Gaussian function (solid lines), yielding 2 pairs of values for the average V_m ($\bar{V}_1$, $\bar{V}_2$) and V_m SD (σ_{V1}, σ_{V2}). These values are used to estimate analytically, by using *Eqs. 11* and *12*, the mean (g_{e0}, g_{i0}) and SD (σ_e, σ_i) of the conductances underlying network activity. From these, analytic forms of the membrane potential distributions, *Eq. 9*, characterizing subthreshold membrane dynamics attributed to synaptic activity can be obtained.

protocol), 2 synaptic noise parameters can be extracted, such as the ratios between excitatory and inhibitory mean and SD. The V_m distributions stemming from 3 injected current levels (3 current-clamps protocol) allow estimation in addition of the reversal potential of either excitatory or inhibitory conductances. Alternatively, multiple current clamps (≥ 3) can be used as consistency conditions for validating the obtained estimates. However, in what follows we restrict discussion to the 2 current-clamps protocol.

Test of the approach using computational models

We now turn to computational models of increasing levels of complexity to test the conductance estimates provided by *Eqs. 11* and *12*. First, we used the point-conductance model to check for the validity of the expressions obtained. Because of the equivalence of the underlying equations (*Eqs. 1, 2,* and *3*), here the closest correspondence between estimated and actual (i.e., calculated numerically) conductance parameters is expected.

Figure 3 illustrates the procedure applied to the V_m activity of that model (Fig. 3*A*). Two different values of steady current injection (I_{ext1} and I_{ext2}) yield 2 V_m distributions (Fig. 3*B*, gray). These distributions were fitted with a Gaussian function to obtain the means and SDs of the membrane potential at both current levels. Incorporating the values $\bar{V}_1$, $\bar{V}_2$, σ_{V1}, and σ_{V2} into *Eqs. 11* and *12* yields values for the mean and SD of the synaptic noise, $g_{\{e,i\}0}$ and $\sigma_{\{e,i\}}$, respectively (Fig. 3*C*, solid line, and Fig. 3*D*). These estimates were then used to recon-

struct the full analytic expression of the V_m distribution using *Eq. 9,* which was plotted in Fig. 3*B* (solid lines). There was a very close match between the analytic estimates of $\rho(V)$ and numerical simulations (Fig. 3*B,* compare gray areas with solid lines). This demonstrates not just that Gaussian distributions are an excellent approximation for the membrane potential distribution in the presence of synaptic noise, but also that the proposed method yields an excellent characterization of the synaptic noise and thus subthreshold neuronal activity. This can also be seen by comparing the reconstructed conductance distributions (Fig. 3*C,* solid lines) with the actual conductances recorded during the numerical simulation (Fig. 3*C,* gray). Distributions deduced from the estimated parameters were in excellent agreement with those of the numerical simulations. Thus, this first set of simulations shows that, at least for the point-conductance model, the proposed approach provides a method that allows an accurate estimate of the mean and the variance of synaptic conductances from the sole knowledge of the (subthreshold) membrane potential activity of the cell.

A second test was to apply this method to a more realistic model of synaptic noise, in which synaptic activity was generated by a large number of individual synapses releasing randomly according to Poisson processes (see Fig. 1*B*). An example of the application of the procedure to this type of model is shown in Fig. 4. Starting from the V_m activity (Fig. 4*A*), membrane potential distributions were constructed and fitted by Gaussians for 2 levels of injected current (Fig. 4*B,* gray). Estimates of the mean and variance of excitatory and inhibitory conductances were then obtained using *Eqs. 11* and *12*. The analytic solution reconstructed from this estimate (Fig. 4*B,* solid lines) is in excellent agreement with the numerical
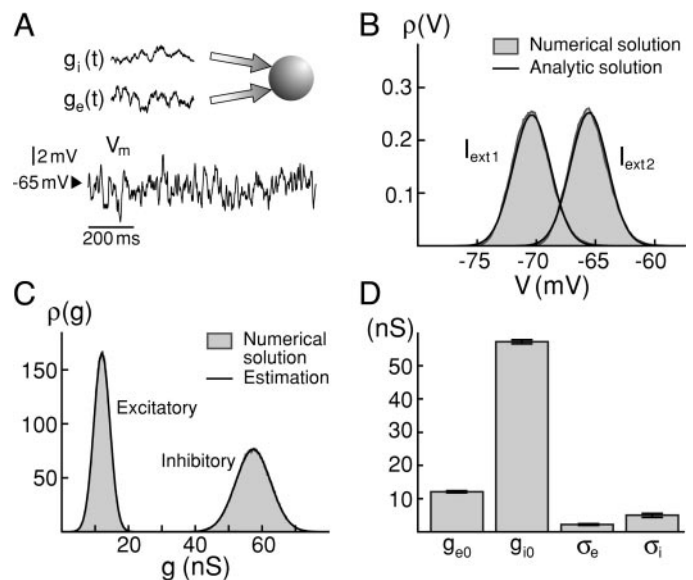

FIG. 3. Test of the method for estimating synaptic conductances using the point-conductance model. *A*: example of membrane potential (V_m) dynamics of the point-conductance model. *B*: V_m distributions used to estimate synaptic conductances. Those distributions (gray) were obtained at 2 different current levels, I_{ext1} and I_{ext2}. Solid lines indicate the analytic solution based on the conductance estimates. *C*: comparison between the conductance distributions deduced from the numerical solution of the underlying model (gray) with the conductance estimates (solid lines). *D*: bar plot showing the mean and SD of conductances estimated from the membrane potential distributions. Error bars indicate the statistical significance of the estimates by using different Gaussian approximations of the membrane potential distribution in *B*.
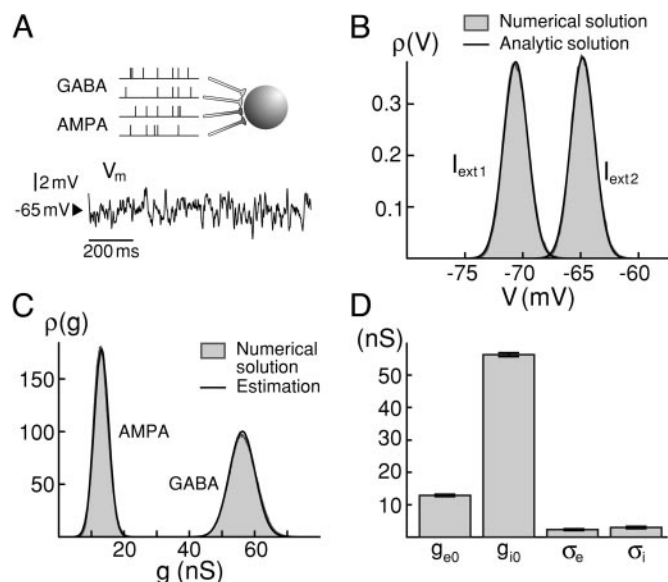
FIG. 4. Estimation of synaptic conductances from analyzing the membrane potential activity in a single-compartment model model with realistic synaptic inputs. *A*: example of membrane potential (V_m) time course in a single-compartment model receiving thousands of randomly activated synaptic conductances (same model as in Fig. 1*B*). *B*: V_m distributions used to estimate conductances. Those distributions are shown at 2 different current levels, I_{ext1}, I_{ext2} (gray). Solid lines indicate the analytic solution obtained based on the conductance estimates. *C*: comparison between the conductance distributions deduced from the numerical solution of the underlying model (gray) with those reconstructed from the estimated conductances (solid lines). *D*: bar plot showing the mean and SD of conductances estimated from membrane potential distributions. Error bars indicate the statistical significance of the estimates by using different Gaussian approximations of the membrane potential distribution in *B*.

simulations of this model. Moreover, the reconstructed conductance distributions based on this estimate (Fig. 4*C*, solid lines) are also in excellent agreement with the total conductance calculated for each type of synapse in the numerical simulations (Fig. 4*C*, gray; see Fig. 4*D* for quantitative values and error estimates). Thus, also in case of this more realistic model of synaptic background activity, which markedly differs from the point-conductance model, the estimates of synaptic conductances and their variances from voltage distributions are in excellent agreement with the values obtained numerically. In fact, this agreement can be expected because of the close correspondence between the conductance dynamics in both models (see Fig. 1, *C–E*).

A third, more severe test was to apply this estimate to a compartmental model in which individual (random) synaptic inputs were spatially distributed in soma and dendrites. In a passive model of a cortical pyramidal neuron from layer VI (Fig. 5*A*; see METHODS), the V_m distributions obtained at 2 steady current levels were approximately symmetric (Fig. 5*B*, *left panel*, gray). Again, applying *Eqs. 11* and *12* to estimate synaptic conductances and their variances led to analytic V_m distributions $\rho(V)$ (Fig. 5*B*, *left panel*, solid lines), which captured very well the shape of the V_m distributions obtained numerically, although small deviations are visible at the hyperpolarized and depolarized tail of the distributions. The reconstructed conductance distributions (Fig. 5*C*, solid lines) were also in excellent agreement with the conductance distributions obtained in this model using an ideal voltage clamp at the soma (Fig. 5*C*, gray; see

method in Destexhe et al. 2001). The quantitative comparison of those values (Fig. 5*D*, *left panel*) shows that the estimation from V_m distributions gives comparable estimates as the ideal voltage clamp. This agreement also shows that the dendritic filtering of synaptic inputs, caused by the spatial extension of the dendritic tree, does have only a minor impact on the conductance estimation. Moreover, because of the higher density of GABAergic synapses in the proximal region of cortical neurons, a slight bias in the estimates toward inhibitory conductance is expected. However, our results indicate that this effect is small and has only a minimal impact on the overall conductance estimates.

Finally, by incorporating voltage-dependent currents (I_{Na}, I_{Kd} for spike generation, and a slow voltage-dependent K^+ current for spike-frequency adaptation, a hyperpolarization-activated current I_h, a low-threshold Ca^{2+} current I_{CaT}, and an A-type K^+ current I_{KA} with densities typical for cortical neurons; see METHODS) in the detailed biophysical model, we probed the applicability of the proposed method to more realistic situations with active dendrites capable of generating and conducting dendritic spikes. Here, deviations are expected because the method is strictly based on passive neuronal dynamics (see *Eq. 1*), which might be strongly altered by the presence of active channels at the site of the recording and the presence of regenerative dendritic spikes. Indeed, after removing spikes in a broad (10-ms) time window, the subthreshold activity approximated the passive dynamics, but showed deviations in the membrane potential distribution at its hyperpolarized and depolarized tails (Fig. 5*B*, gray, compare *left* and *right*). However, these deviations had only a minimal impact on the mean and variance of the membrane potential obtained by Gaussian fits, which constitute the input for the VmD method. Applying *Eqs. 11* and *12* led to estimates (Fig. 5*B*, *right panel*, solid lines) that showed more significant—albeit still small—deviations from the distributions drawn from the corresponding numerical simulations (Fig. 5*B*, *right panel*, gray; Fig. 6, gray). In general, the estimated values for synaptic conductances and their variance showed larger errors, especially for σ_i (Fig. 5*D*, *right panel*), and yielded V_m distributions that were slightly broader. However, these errors and deviations remained relatively small and the method still provided a good estimate of synaptic conductances, similar to or better than the one provided by ideal voltage clamp (Fig. 6).

Test of the method using in vitro recordings and dynamic-clamp experiments

The method was further tested against real network activity. We used the recurrent activity ("up-states") occurring spontaneously in ferret neocortical slices (see METHODS). Intracellularly, this activity consists in a depolarized V_m and relatively large-amplitude V_m fluctuations (Fig. 7), as described previously (Sanchez-Vives and McCormick 2000). To test the method, we applied an on-line protocol (Fig. 7*A*), consisting of estimating synaptic conductances from "natural" up-states (*top traces*) and compared them to "artificial" up-states obtained by dynamic-clamp injection of the estimated conductances in the same neuron (*bottom traces*). As above, the estimates (Fig. 7*A*, solid distributions) were obtained by computing the V_m distributions at 2 different current levels (Fig. 7*A*, *top*, gray distri-
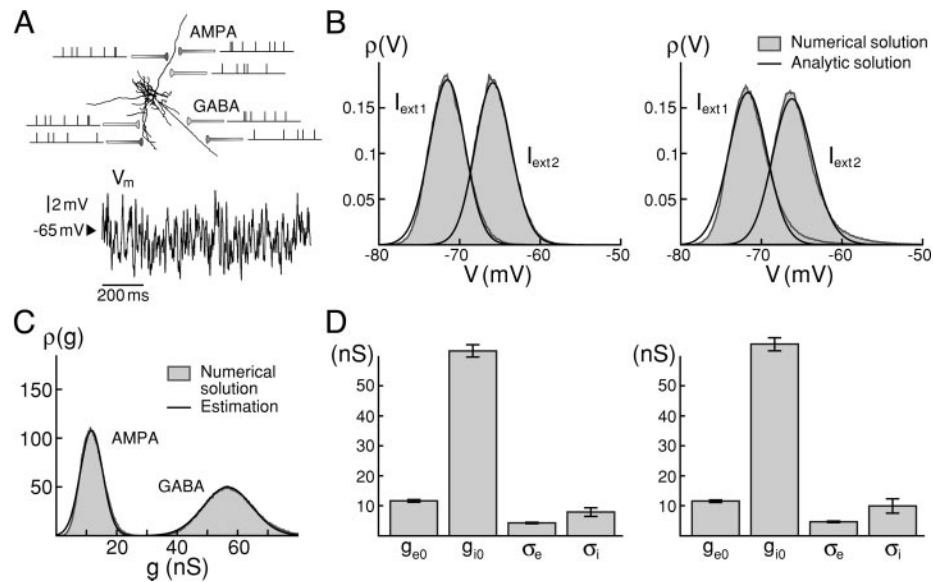
FIG. 5. Estimation of synaptic conductances from the membrane potential activity of a detailed biophysical model of synaptic background activity. *A*: example of the membrane potential (V_m) activity obtained in a detailed biophysical model of a layer VI cortical pyramidal neuron (scheme on *top;* same model as in Destexhe and Paré 1999). Synaptic background activity was modeled by the random release of 16,563 AMPA-mediated and 3,376 GABA$_A$-mediated synapses distributed in dendrites according to experimental measurements. *B*: V_m distributions obtained in this model at 2 different current levels, I_{ext1} and I_{ext2}. *Left panel:* distributions obtained in a passive model. *Right panel:* distributions obtained are shown when the model had active dendrites (Na$^+$ and K$^+$ currents responsible for action potentials and spike-frequency adaptation, located in soma, dendrites, axon). In both cases, results from the numerical simulations (gray) and analytic expression (solid lines), obtained by using the conductance estimates, are shown. *C*: histogram of the total excitatory and inhibitory conductances obtained from the model using an ideal voltage clamp (gray), compared to the distributions reconstructed from the conductance estimates based on V_m distributions. *D*: bar plot showing the mean and SD of synaptic conductances estimated from V_m distributions. Error bars indicate the statistical significance of the estimates by using different Gaussian approximations of the membrane potential distribution in *B*. *Left panel:* passive model; *right panel:* model with voltage-dependent conductances. Presence of voltage-dependent conductances had minor (<10%) effects on the estimated conductance values.

butions) and fit them using the Gaussian approximation (*Eqs. 11* and *12*). For the particular neuron shown in Fig. 7*A*, the estimated inhibitory synaptic conductance parameters were approximately twice as large as those for excitation (see *bottom bar plots*). These parameters were then used to generate conductance waveforms according to the stochastic process of *Eq. 3* ("Model of synaptic noise" in Fig. 7*A*). These conductance waveforms were then reinjected in the same neuron ("Dynamic-clamp" in Fig. 7*A*), leading to re-created up-states, which are compared to natural up-states. In several cells tested ($n = 4$), the re-created states had properties (average V_m, V_m fluctuations, firing behavior) similar to those of the natural up-states (see example in Fig. 7*B*).

Such a comparison is shown in more detail in Fig. 8*A*. The natural up-states (Fig. 8*A, top trace*) were used to estimate conductances using the same procedure as in Fig. 7*A*. In the particular cell shown in Fig. 8, excitatory and inhibitory conductances were approximately equal, but the variance of inhibitory conductance was relatively high (see *bar plot*). These estimated values for g_{e0}, g_{i0}, σ_e, and σ_i were then used to generate stochastic conductance waveforms (Fig. 8*A, bottom traces*). Injection of these conductance waveforms during quiescent states into the same cell led to artificial up-states, in which V_m distribution was in excellent agreement with the natural up-states [see $\rho(V)$ graph in Fig. 8*A*]. This dynamic-clamp protocol shows that the network activity, as predicted by the V_m distribution method, is perfectly consistent with the natural network activity.

An alternative way for testing the V_m distribution method is to analyze artificial up-states generated by dynamic-clamp injection of known conductances (Fig. 8*B*). In this case, we injected stochastic conductance waveforms according to a predefined choice of g_{e0}, g_{i0}, σ_e, and σ_i parameters. The artificial up-states obtained were then analyzed using the VmD decomposition method. This procedure led to estimated values in excellent agreement with the injected values (compare light and dark gray in *bar plot* of Fig. 8*B*). Thus, the method provides an acceptable estimate of the injected conductances from the sole knowledge of the V_m activity.

DISCUSSION

In this paper, we have provided a theoretical description of the subthreshold membrane potential activity of neurons under synaptic bombardment, and provided means to estimate the underlying global characteristics of network activity. We discuss here the advantages and problems of this approach, how it relates to previous work, and what perspectives are expected.

Starting from a purely theoretical approach, the mathematical description of the stochastic variations of V_m, we derived expressions to relate V_m measurements to global synaptic conductance parameters, such as the mean excitatory (g_{e0}) and inhibitory (g_{i0}) conductances, as well as their respective variances (σ_e, σ_i). The mean synaptic conductances are related to the mean rate of afferent neurons, whereas the variances of these conductances are related to the level of correlation between presynaptic activities (Destexhe et al. 2001). So far, experimental measurements have concentrated on estimating
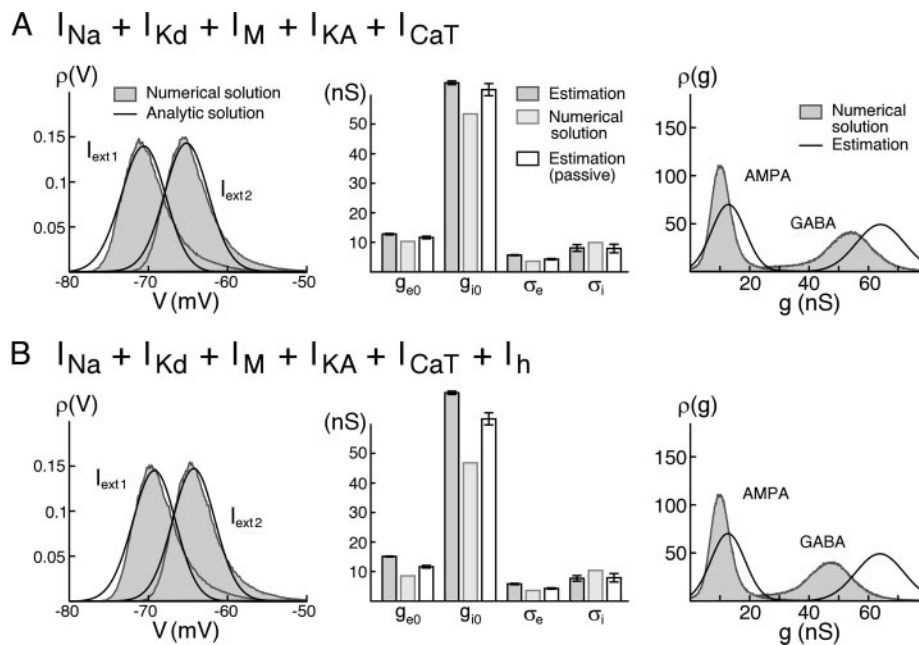
FIG. 6.   Estimation of synaptic conductances from the membrane potential activity in detailed biophysical models with active dendrites. *A*: model with voltage-dependent currents for spike generation (I_{Na}, I_{Kd}), spike-frequency adaptation (I_M), A-type K^+ current (I_{KA}) and low-threshold Ca^{2+} current (I_{CaT}) in soma and dendrites. *B*: model with additional hyperpolarization-activated current I_h in soma and dendrites (see METHODS). In both cases, synaptic background activity was modeled by the random release of 16,563 AMPA-mediated and 3,376 GABA$_A$-mediated synapses distributed in dendrites according to experimental measurements. *Left panels:* V_m distributions at 2 different current levels (I_{ext1} and I_{ext2}) obtained numerically (gray) and analytically using conductance estimates obtained with the VmD method. Comparison of the conductance estimates obtained with the VmD method (*middle panels,* dark gray bars; *A*: g_{e0} = 12.8 nS, g_{i0} = 64.0 nS, σ_e = 5.7 nS, σ_i = 8.1 nS; *B*: g_{e0} = 15.1 nS, g_{i0} = 70.4 nS, σ_e = 5.8 nS, σ_i = 7.7 nS) and ideal somatic voltage-clamp (*middle panels,* light gray bars; Gaussian fits yield *A*: g_{e0} = 10.3 nS, g_{i0} = 53.4 nS, σ_e = 3.6 nS, σ_i = 9.9 nS; *B*: g_{e0} = 8.3 nS, g_{i0} = 46.8 nS, σ_e = 3.6 nS, σ_i = 10.3 nS) shows that the VmD method gave results that were much closer to the true values of synaptic conductances seen in the corresponding passive model (*middle panels,* white bars; g_{e0} = 11.6 nS, g_{i0} = 61.7 nS, σ_e = 4.3 nS, σ_i = 7.9 nS; see also Fig. 5). *Right panels:* comparison of histograms of the total excitatory and inhibitory conductances obtained numerically using ideal somatic voltage-clamp (gray) and the Gaussian distribution based on the estimates using the VmD method.

the mean conductances (Anderson et al. 2000; Borg-Graham 1998; Hirsch et al. 1998; Shu et al. 2003a), which is equivalent to estimating the mean level of afferent activity. Measuring conductance variances can give estimates of the mean level of correlation within afferent activity (Destexhe et al. 2001). However, such estimates were never provided so far, presumably because of the technical difficulty of measuring conductance variances in vivo, which presently requires voltage-clamp methods.

The present V_m distribution method provides such estimates based on current-clamp recordings. It relies on quantities (mean and variance of the V_m), which are relatively easy to measure experimentally. Conductances are usually best estimated from voltage-clamp recordings (Borg-Graham et al. 1998), although methods from current-clamp recordings have been used as well (Anderson et al. 2000; Hirsch et al. 1998). The method proposed here relies on standard current-clamp protocols, in which spontaneous activity is recorded with steady current injection, which corresponds to the most current configuration used for performing intracellular recordings in vivo.

We have shown that the method can provide relatively good estimates of global synaptic conductances, even in the case of complex models, including the dendritic morphology and active channels in dendrites (Fig. 5). In the latter case, the method provides measurements of global conduc-

tances and their variances with an accuracy comparable to that of an "ideal" voltage clamp. However, it must be noted that the method we used here to estimate conductance variances from voltage clamp required running the models twice with the same seed for random numbers. On the contrary, the proposed VmD method provides such an estimate without requirements of this type.

On the negative side, the method proposed here to estimate conductance variances relies on a series of parameters. First, there must be an estimation of the "effective" leak conductance (i.e., the nonsynaptic conductance) and membrane area *a*. These values can be obtained in vitro by measuring the input resistance and time constant in quiescent periods (see METHODS). Second, voltage-dependent currents in soma and dendrites may distort the V_m distribution and cause errors in the estimate, attributed to either the presence of regenerative dendritic spikes or the activation of voltage-dependent membrane conductances. The latter applies to all currents that are active in the subthreshold V_m range, such as the hyperpolarization-activated current I_h. Slow K^+ currents may also be activated in the subthreshold range, although in our simulations (Fig. 5) there were slow K^+ currents, but their presence did not seem to have strong effects on the estimates. Various K^+ currents (such as those underlying spike afterhyperpolarization or the A-type K^+ current I_{KA}), various Ca^{2+} currents (such as the low-threshold T-current I_{CaT}), or I_h may also significantly distort
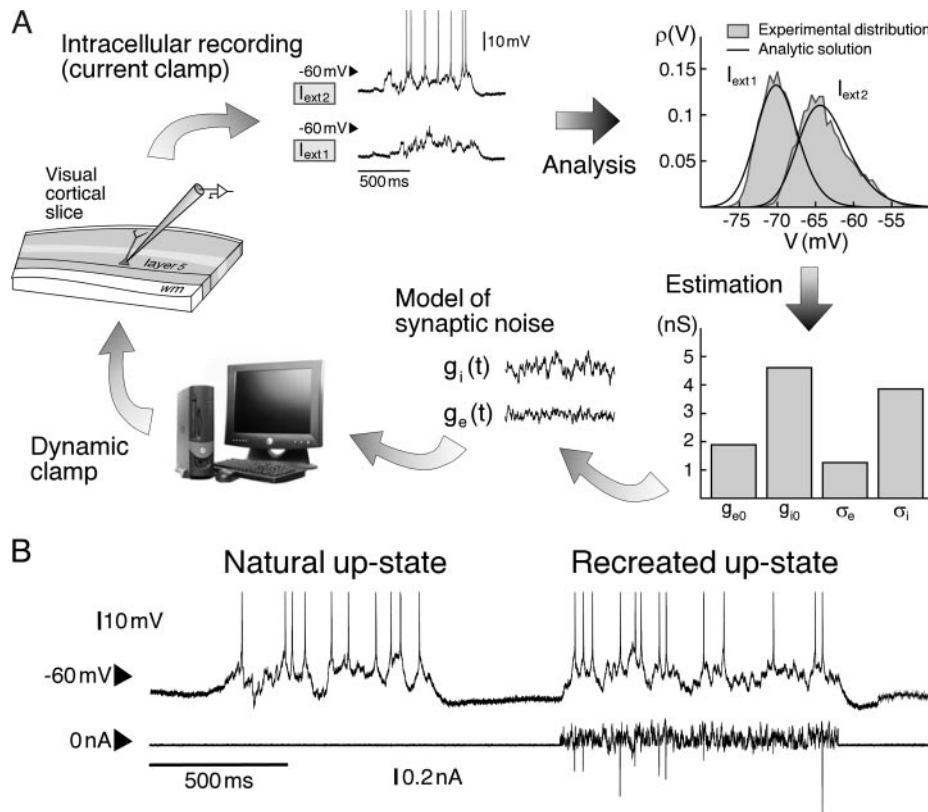
FIG. 7. Estimation of synaptic conductances from active states in vitro and dynamic-clamp re-creation of active states. *A*: sketch of the procedure for conductance estimation and test of the estimates. *Top left:* spontaneous active network states ("up-states") were recorded intracellularly in ferret visual cortex slices at 2 different injected current levels (I_{ext1}, I_{ext2}). *Top right:* V_m distributions (gray) were computed from experimental data and used to estimate synaptic conductances. Analytic solution for the V_m distribution using those conductance estimates is shown by solid lines. *Bottom right:* histogram of the mean and SD of excitatory and inhibitory conductances obtained from the fitting procedure. *Bottom left:* a dynamic-clamp protocol was used to inject stochastic conductances consistent with these estimates, therefore re-creating artificial up-states in the same neuron. *B*: example of natural and re-created up-states in the same cell as in *A*. This procedure re-created V_m activity similar to the active state, as shown by the close matching of the V_m fluctuations, depolarized level, and discharge variability (natural up-states: $\bar{V} = -67.2$ mV, $\sigma_v = 3.06$ mV, firing rate 14.3 Hz; re-created up-states: $\bar{V} = -66.96$ mV, $\sigma_v = 2.6$ mV, firing rate 13 Hz).

the V_m distribution (see Fig. 6), but the distorting effect of these currents can easily be avoided (see METHODS). Moreover, as our numerical simulations showed, despite a significant impact of these active currents, the estimates obtained with the VmD method were closer to the actual synaptic conductances compared to estimates with ideal voltage clamp. However, to minimize voltage-dependent effects, the best is to identify a linear region of the *I–V* curve of the neuron, and perform the measurements in that region. The excellent agreement obtained here using experimental recordings (Fig. 8) also suggests that these contaminations are minimal in the voltage range considered. Furthermore, using Gaussian fits of the V_m distributions effectively suppresses the effect of dendritic spikes arriving at the site of the recording and, thus, improves the applicability of the method. Third, the presented VmD method restricts, so far, only to glutamatergic and $GABA_A$ receptors. The impact of other receptor types, such as $GABA_B$ and NMDA, remains to be investigated and neglecting them might contribute to errors in the conductance estimates. Moreover, the knowledge of the reversal potential for GABAergic or glutamatergic synapses is crucial and using wrong values of reversals will result in estimation errors. Ideally, the reversal potentials should be measured for the same preparation in which the analysis is made. Finally, drifts in the membrane potential (e.g., arising from the experimental setup or from unstability of the recording) constitute another source of error. The proposed method requires a stationary recording, which was the case for all cells shown here.

Another potential source of error comes from the spatial aspect of synaptic noise. Here, synaptic inputs received distally will contribute less to the somatic response compared to those close to the soma. This will, in general, result in an underes-

timation of the total synaptic conductances and their variation. Moreover, a nonuniform distribution of synaptic conductances, such as the higher density of GABAergic synapses in the proximal region of cortical neurons, or the distance-dependent scaling of quantal conductances or receptor number, will bias the estimates for excitatory and inhibitory conductances. However, our simulations, which took the spatial distribution of (uniform) synaptic channels and the asymmetry in the distribution of glutamatergic and GABAergic synapses into account, showed only minimal deviations from the corresponding voltage-clamp estimates of the excitatory and inhibitory synaptic conductances. In addition, our method yields estimates for the total synaptic conductances that determine the cellular dynamics at the site of the recording, a quantity that does not depend on a specific assumption of the distribution of synaptic channels within the dendritic tree.

This approach is also applicable to in vivo intracellular experiments. In this case, the mean and variance of synaptic conductances could be estimated across different states of the network. The difficulty, however, would be to estimate the resting parameters (g_L, a), which are not easy to deduce in vivo. However, if quiescent states can be obtained either pharmacologically (Paré et al. 1998) or spontaneously ("down-states"), then estimates of those parameters can be obtained. Alternatively, it is always possible to use the present approach with minor modifications to estimate relative changes of conductances or conductance variances between different states of the network. In particular, measuring changes in conductance variances should allow us to measure changes in correlation in network activity. Such measurements have not been obtained yet, but should be possible in the near future.
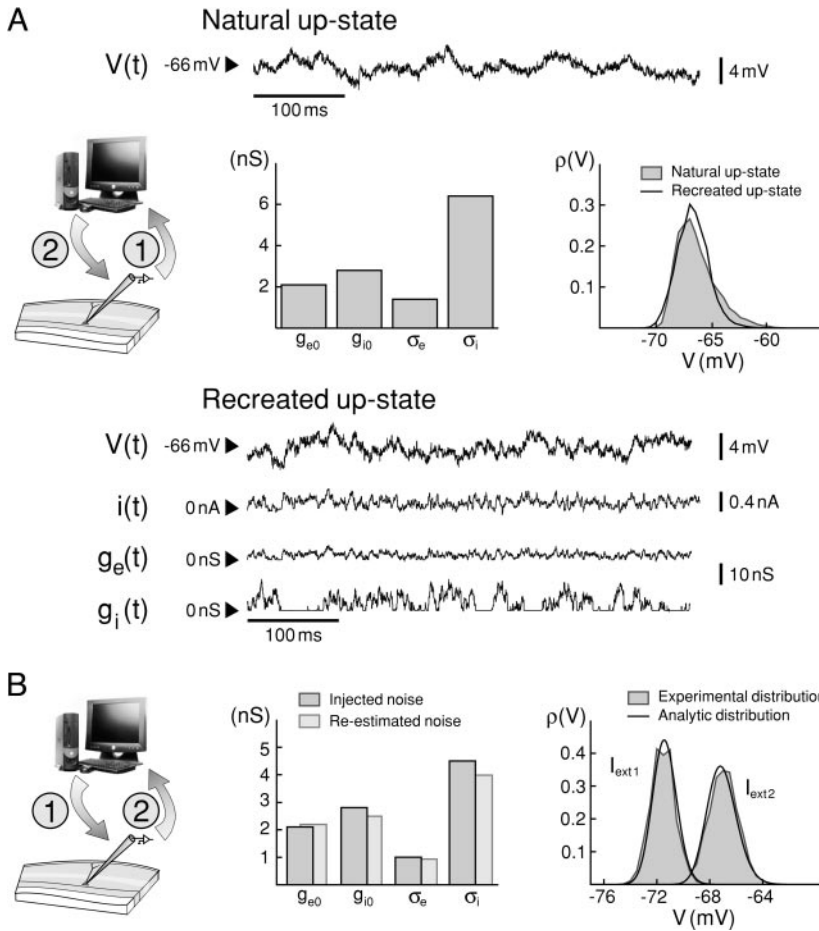
A

B

FIG. 8. Test of the method using natural and re-created up-states in vitro under dynamic clamp. *A*: reinjection of conductance estimates. Protocol used was similar as in Fig. 7 and consisted in first extracting conductances from natural up-states (arrow 1 in scheme) and re-creating artificial up-states in the same neuron (arrow 2). The natural up-states (*top trace*) were used to compute V_m distribution and estimate conductances (*middle panels,* gray). These values were then used to generate artificial synaptic noise using stochastically fluctuating conductances (g_e and g_i), which were injected in the same neuron using dynamic clamp [V_m activity shown as $V(t)$ in *bottom traces*]. V_m distributions obtained were in excellent agreement (gray: natural up-states, $\bar{V} = -66.87$ mV, $\sigma_V = 1.53$ mV; continuous line: re-created up-states, $\bar{V} = -66.81$ mV, $\sigma_V = 1.36$ mV). *B*: analysis of artificial up-states produced by dynamic-clamp injection of known conductances. In this protocol, stochastically varying synaptic conductances were first injected in the neuron (arrow 1 in scheme). Resulting V_m activity was then used to reestimate the conductances (arrow 2). *Middle panel:* injected (dark gray) and reestimated (light gray) conductances. *Right panel:* corresponding V_m distributions (gray: experimental; solid lines: analytic prediction from the reestimated parameters). There was an excellent agreement between all values (injected conductances: $g_{e0} = 2.1$ nS, $g_{i0} = 2.8$ nS, $\sigma_e = 1.0$ nS, $\sigma_i = 4.5$ nS; reestimated conductances: $g_{e0} = 2.2$ nS, $g_{i0} = 2.5$ nS, $\sigma_e = 0.94$ nS, $\sigma_i = 4.0$ nS).

APPENDIX

In this appendix we briefly summarize the mathematical approach for deducing the steady-state membrane potential distributions of the stochastic passive membrane equation (*Eqs. 1–3*) describing the subthreshold membrane dynamics in the presence of synaptic noise.

The Fokker–Planck equation

The stochastic passive membrane equation given in *Eqs. 1–3* was analytically accessed within the framework of the stochastic differential calculus (Gardiner 2002; Mortensen 1969; van Kampen 1981). Here, using a set of differential rules (Itô rules) for the OU stochastic process allows deduction of the Fokker–Planck equation (Risken 1984), corresponding to the set of stochastic differential equations (*Eqs. 1–3*)

$$\partial_t \rho(V, t) = -\partial_V[f(V)\rho(V, t)] + \partial_V\{h_e(V)\partial_V[h_e(V)\alpha_e(t)\rho(V, t)]\}$$
$$+ \partial_V\{h_i(V)\partial_V[h_i(V)\alpha_i(t)\rho(V, t)]\} \quad (A1)$$

where

$$f(V) = \frac{1}{aC_m}[I_{\text{ext}} - ag_L(V - E_L) - g_{e0}(V - E_e) - g_{i0}(V - E_i)] \quad (A2)$$

is a voltage-dependent drift term, $h_{\{e,i\}}(V) = -(V - E_{\{e,i\}})/(aC_m)$ are voltage-dependent excitatory and inhibitory conductances noise terms, and

$$2\alpha_{\{e,i\}}(t) = \sigma_{\{e,i\}}^2 \tilde{\tau}_{\{e,i\}}(1 - e^{-t/\tilde{\tau}_{\{e,i\}}}) + \frac{1}{2\tilde{\tau}_{\{e,i\}}}\tilde{w}_{\{e,i\}}^2(t) - \sigma_{\{e,i\}}^2 t \quad (A3)$$

where $\tilde{w}_{\{e,i\}}(t) = \int_0^t ds\, sg_{\{e,i\}}(s)$ are the integrated stochastic processes for the stochastic conductances $g_{\{e,i\}}$, and $\tilde{\tau}_{\{e,i\}}$ denote effective noise time constants given by $\tilde{\tau}_{\{e,i\}} = 2\tau_{\{e,i\}}\tau_0/\tau_{\{e,i\}} + \tau_0)$, with $\tau_0 = aC_m/(ag_L + g_{e0} + g_{i0})$. The Fokker–Planck equation (*Eq. A1*) describes the time evolution of the probability density function $\rho(V, t)$ of the membrane potential $V(t)$ in the presence of excitatory and inhibitory synaptic noise terms characterized by their mean and variances.

The steady-state membrane potential distribution

In the limit $t \to \infty$, the Fokker–Planck equation (*Eq. A1*) can be solved analytically. In this case, one obtains the *steady-state probability distribution* $\rho(V)$ for the membrane potential V

$$\rho(V) = N\exp\left\{A_1\ln\left[\frac{u_e(V - E_e)^2}{(aC_m)^2} + \frac{u_i(V - E_i)^2}{(aC_m)^2}\right]\right.$$
$$\left. + A_2\arctan\left[\frac{u_e(V - E_e) + u_i(V - E_i)}{(E_e - E_i)\sqrt{u_e u_i}}\right]\right\} \quad (A4)$$

where the following constants are defined: $k_L = 2a^2C_m g_L$, $k_e = 2aC_m g_{e0}$, $k_i = 2aC_m g_{i0}$, $u_e = \sigma_e^2\tilde{\tau}_e$, and $u_i = \sigma_i^2\tilde{\tau}_i$, as well as the following voltage-independent terms

$$A_1 = -\frac{k_L + k_e + k_i + u_e + u_i}{2(u_e + u_i)}$$

and

$$A_2 = 2aC_m \frac{\begin{array}{c}(g_{e0}u_i - g_{i0}u_e)(E_e - E_i) - ag_L u_e(E_e - E_L) \\ - ag_L u_i(E_i - E_L) + I_{\text{ext}}(u_i + u_e)\end{array}}{(E_e - E_i)\sqrt{u_e u_i}(u_e + u_i)}$$

where N denotes a normalization constant such that $\int_{-\infty}^{\infty} dV \rho(V) = 1$. The matching of this analytic solution and the numerical simulations are illustrated in Fig. 1*E* (dashed lines; see Rudolph and Destexhe 2003b for details).

Gaussian approximation of the steady-state membrane potential distribution

Because of the multiplicative coupling of the stochastic conductances to the membrane potential in I_{syn}, the membrane potential probability distribution (*Eq. A4*) takes in general an asymmetric form. However, $\rho(V)$ shows only small deviations from a Gaussian distribution, suggesting an approximation by a symmetric distribution. To this end, the exponent in *Eq. A4* was replaced by the 2 first-order terms of its Taylor expansion around the maximum $\bar{V}$ of the probability distribution $\rho(V)$

$$\bar{V} = \frac{S_1}{S_0} \tag{A5}$$

with $S_0 = k_L + k_e + k_i + u_e + u_i$ and $S_1 = k_L E_L + k_e E_e + k_i E_i + u_e E_e + u_i E_i + 2a C_m I_{ext}$. This yields the following Gaussian distribution

$$\rho(V) = \frac{1}{\sqrt{2\pi\sigma_V^2}} \exp\left[-\frac{(V - \bar{V})^2}{2\sigma_V^2}\right] \tag{A6}$$

with the SD given by

$$\sigma_V^2 = \frac{S_0^2(u_e E_e^2 + u_i E_i^2) - 2 S_0 S_1 (u_e E_e + u_i E_i) + S_1^2(u_e + u_i)}{S_0^3} \tag{A7}$$

Using 2 levels of (constant) injected current I_{ext}, these relations can be inverted (see *Eqs. 11* and *12* and details in text), yielding estimates for the mean and variance of synaptic conductances.

REFERENCES

Anderson JS, Carandini M, and Ferster D. Orientation tuning of input conductance, excitation, and inhibition in cat primary visual cortex. *J Neurophysiol* 84: 909–926, 2000.

Bekkers JM. Properties of voltage-gated potassium currents in nucleated patches from large layer 5 cortical pyramidal neurons of the rat. *J Physiol* 525: 593–609, 2000.

Bernander O, Douglas RJ, Martin KA, and Koch C. Synaptic background activity influences spatiotemporal integration in single pyramidal cells. *Proc Natl Acad Sci USA* 88: 11569–11573, 1991.

Borg-Graham LJ, Monier C, and Frégnac Y. Visual input evokes transient and strong shunting inhibition in visual cortical neurons. *Nature* 393: 369–373, 1998.

Braitenberg V and Schüz A. *Cortex: Statistics and Geometry of Neuronal Connectivity* (2nd ed.). Berlin: Springer-Verlag, 1998.

Chance FS, Abbott LF, and Reyes AD. Gain modulation from background synaptic input. *Neuron* 15: 773–782, 2002.

Contreras D and Steriade M. Cellular basis of EEG slow rhythms: a study of dynamic corticothalamic relationships. *J Neurosci* 15: 604–622, 1995.

Contreras D, Destexhe A, and Steriade M. Intracellular and computational characterization of the intracortical inhibitory control of synchronized thalamic inputs in vivo. *J Neurophysiol* 78: 335–350, 1997.

Creutzfeldt O, Watanabe S, and Lux HD. Relation between EEG phenomena and potentials of single cortical cells. I. Evoked responses after thalamic and epicortical stimulation. *EEG Clin Neurophysiol* 20: 1–18, 1966a.

Creutzfeldt O, Watanabe S, and Lux HD. Relation between EEG phenomena and potentials of single cortical cells. II. Spontaneous and convulsoid activity. *EEG Clin Neurophysiol* 20: 19–37, 1966b.

DeFelipe J and Fariñas I. The pyramidal neuron of the cerebral cortex: morphological and chemical characteristics of the synaptic inputs. *Prog Neurobiol* 39: 563–607, 1992.

Destexhe A, Badoual M, Piwkowska Z, Bal T, Hasenstaub A, Shu Y, McCormick DA, Pelletier J, Paré D, and Rudolph M. In vivo, in vitro and computational evidence for balanced or inhibition-dominated network states, and their respective impact on the firing mode of neocortical neurons. *Soc Neurosci Abstr* 29: 921. 14, 2003.

Destexhe A, Mainen Z, and Sejnowski TJ. Kinetic models of synaptic transmission. In: *Methods in Neuronal Modeling,* edited by Koch C and Segev I. Cambridge, MA: MIT Press, 1998, p. 1–26.

Destexhe A and Paré D. Impact of network activity on the integrative properties of neocortical pyramidal neurons in vivo. *J Neurophysiol* 81: 1531–1547, 1999.

Destexhe A, Rudolph M, Fellous JM, and Sejnowski TJ. Fluctuating conductances recreate in-vivo-like activity in neocortical neurons. *Neuroscience* 107: 13–24, 2001.

Destexhe A, Rudolph M, and Paré D. The high-conductance state of neocortical neurons *in vivo. Nat Rev Neurosci* 4: 739–751, 2003.

Evarts EV. Temporal patterns of discharge of pyramidal tract neurons during sleep and waking in the monkey. *J Neurophysiol* 27: 152–171, 1964.

Fellous JM, Rudolph M, Destexhe A, and Sejnowski TJ. Synaptic background noise controls the input/output characteristics of single cells in an in vitro model of in vivo activity. *Neuroscience* 122: 811–829, 2003.

Gardiner CW. *Handbook of Stochastic Methods.* Berlin: Springer-Verlag, 2002.

Gutfreund Y, Yarom Y, and Segev I. Subthreshold oscillations and resonant frequency in guinea-pig cortical neurons: physiology and modelling. *J Physiol* 483: 621–640, 1995.

Hamill OP, Huguenard JR, and Prince DA. Patch-clamp studies of voltage gated currents in identified neurons of the rat cerebral cortex. *Cereb Cortex* 1: 48–61, 1991.

Hines ML and Carnevale NT. The NEURON simulation environment. *Neural Comput* 9: 1179–1209, 1997.

Hirsch JA, Alonso JM, Clay Reid R, and Martinez LM. Synaptic integration in striate cortical simple cells. *J Neurosci* 18: 9517–9528, 1998.

Hô N and Destexhe A. Synaptic background activity enhances the responsiveness of neocortical pyramidal neurons. *J Neurophysiol* 84: 1488–1496, 2000.

Hodgkin AL and Huxley AF. A quantitative description of membrane current and its application to conduction and excitation in nerve. *J Physiol* 117: 500–544, 1952.

Huguenard JR, Hamill OP, and Prince DA. Developmental changes in Na^+ conductances in rat neocortical neurons: appearance of a slowly inactivating component. *J Neurophysiol* 59: 778–795, 1988.

Klee MR, Offenloch K, and Tigges J. Cross-correlation analysis of electroencephalographic potentials and slow membrane transients. *Science* 147: 519–521, 1965.

Migliore M, Hoffman DA, Magee JC, and Johnston D. Role of an A-type K^+ conductance in the back-propagation of action potentials in the dendrites of hippocampal pyramidal neurons. *J Comp Neurosci* 7: 5–15, 1999.

Mortensen RE. Mathematical problems of modeling stochastic nonlinear dynamical systems. *J Stat Phys* 1: 271–296, 1969.

Paré D, Shink E, Gaudreau H, Destexhe A, and Lang EJ. Impact of spontaneous synaptic activity on the resting properties of cat neocortical neurons in vivo. *J Neurophysiol* 79: 1450–1460, 1998.

Prescott SA and De Koninck Y. Gain control of firing rate by shunting inhibition: roles of synaptic noise and dendritic saturation. *Proc Natl Acad Sci USA* 100: 2076–2081, 2003.

Press WH, Flannery HP, Teukolsky SA, and Vetterling WT. *Numerical Recipes. The Art of Scientific Computing.* Cambridge, UK: Cambridge Univ. Press, 1993.

Risken H. *The Fokker Planck Equation: Methods of Solution and Application.* Berlin: Springer-Verlag, 1984.

Robinson HP and Kawai N. Injection of digitally synthesized synaptic conductance transients to measure the integrative properties of neurons. *J Neurosci Methods* 49: 157–165, 1993.

Rudolph M and Destexhe A. A method to extract the magnitude and variance of synaptic conductances from intracellular recordings in vivo. *Soc Neurosci Abstr* 28: 763.6, 2002.

Rudolph M and Destexhe A. A fast-conducting, stochastic integrative model for neocortical neurons in vivo. *J Neurosci* 23: 2466–2476, 2003a.

Rudolph M and Destexhe A. Characterization of subthreshold voltage fluctuations in neuronal membranes. *Neural Comput* 15: 2577–2618, 2003b.

Sanchez-Vives MV and McCormick DA. Cellular and network mechanisms of rhythmic recurrent activity in neocortex. *Nat Neurosci* 10: 1027–1034, 2000.

Sharp AA, O'Neil MB, Abbott LF, and Marder E. The dynamic clamp: artificial conductances in biological neurons. *Trends Neurosci* 16: 389–394, 1993.

Shelley M, McLaughlin D, Shapley R, and Wielaard J. States of high conductance in a large-scale model of the visual cortex. *J Comput Neurosci* 13: 93–109, 2002.

Shu Y, Hasenstaub A, Badoual M, Bal T, and McCormick DA. Barrages of synaptic activity control the gain and sensitivity of cortical neurons. *J Neurosci* 23: 10388–10401, 2003b.

Shu Y, Hasenstaub A, and McCormick DA. Turning on and off recurrent balanced cortical activity. *Nature* 423: 288–293, 2003a.

Steriade M. Impact of network activities on neuronal properties in cortico-thalamic systems. *J Neurophysiol* 86: 1–39, 2001.

Stuart G and Spruston N. Determinants of voltage attenuation in neocortical pyramidal neuron dendrites. *J Neurosci* 18: 3501–3510, 1998.

Traub RD, Buhl EH, Gloveli T, and Whittington MA. Fast rhythmic bursting can be induced in layer 2/3 cortical neurons by enhancing persistent Na^+ conductance or by blocking BK channels. *J Neurophysiol* 89: 909–921, 2003.

Traub RD and Miles R. *Neuronal Networks of the Hippocampus.* Cambridge, UK: Cambridge Univ. Press, 1991.

Uhlenbeck GE and Ornstein LS. On the theory of the Brownian motion. *Phys Rev* 36: 823–841, 1930.

van Kampen NG. *Stochastic Processes in Physics and Chemistry.* Amsterdam: North-Holland, 1981.